arXiv:1608.00680v2 [cond-mat.supr-con] 20 Aug 2016

Thermodynamic study of gap structure and pair-breaking effect by magnetic field in the heavy-fermion superconductor $CeCu_2Si_2$

Shunichiro Kittaka,[1] Yuya Aoki,[1] Yasuyuki Shimura,[1] Toshiro Sakakibara,[1] Silvia Seiro,[2,3] Christoph Geibel,[2] Frank Steglich,[2] Yasumasa Tsutsumi,[4] Hiroaki Ikeda,[5] and Kazushige Machida[5]

[1]*Institute for Solid State Physics (ISSP), University of Tokyo, Kashiwa, Chiba 277-8581, Japan*
[2]*Max Planck Institute for Chemical Physics of Solids, 01187 Dresden, Germany*
[3]*Department of Chemistry and Physics of Materials, University of Salzburg, Hellbrunner Str. 34, 5020 Salzburg, Austria*
[4]*Department of Basic Science, University of Tokyo, Tokyo 153-8902, Japan*
[5]*Department of Physics, Ritsumeikan University, Kusatsu 525-8577, Japan*

(Dated: August 23, 2016)

This paper presents the results of specific-heat and magnetization measurements, in particular their field-orientation dependence, on the first discovered heavy-fermion superconductor $CeCu_2Si_2$ ($T_c \sim 0.6$ K). We discuss the superconducting gap structure and the origin of the anomalous pair-breaking phenomena, leading e.g., to the suppression of the upper critical field H_{c2}, found in the high-field region. The data show that the anomalous pair breaking becomes prominent below about 0.15 K in any field direction, but occurs closer to H_{c2} for $H \parallel c$. The presence of this anomaly is confirmed by the fact that the specific-heat and magnetization data satisfy standard thermodynamic relations. Concerning the gap structure, field-angle dependences of the low-temperature specific heat within the *ab* and *ac* planes do not show any evidence for gap nodes. From microscopic calculations in the framework of a two-band full-gap model, the power-law-like temperature dependences of C and $1/T_1$, reminiscent of nodal superconductivity, have been reproduced reasonably. These facts further support multiband full-gap superconductivity in $CeCu_2Si_2$.

PACS numbers: 74.70.Tx, 74.25.Bt, 74.25.Op

I. INTRODUCTION

Pairing mechanism of heavy-fermion superconductors has aroused a considerable interest because of a strong Coulomb repulsion between heavy quasiparticles; the conventional electron-phonon interaction is unlikely to be a pairing glue. It has been generally considered that the strong Coulomb repulsion can be avoided by an unconventional pairing in which the superconducting gap has nodes. Because the nodal structure contains crucial information on the nature of novel pairing glues,[1] determination of the superconducting gap symmetry is of primary importance. For instance, CeMIn$_5$ (M=Co, Rh, Ir) systems have been identified to be $d_{x^2-y^2}$-wave superconductors from field-angle-resolved experiments,[2–6] and spin fluctuations associated with an antiferromagnetic quantum critical point are considered to play an important role in mediating Cooper pairs.

The first heavy-fermion superconductor $CeCu_2Si_2$ discovered in 1979 (Ref. 7) was also considered to be a nodal *d*-wave superconductor mediated by antiferromagnetic spin fluctuations.[8] Indeed, the superconducting ground state (S-type) sensitively transforms to the antiferromagnetic one (A-type) by a slight change in the composition ratio of Cu/Si.[9] In the superconducting state, strong limit of the upper critical field H_{c2} is observed at low temperatures in any field direction. This H_{c2} limit, plausibly originating from the Pauli-paramagnetic effect, and a distinct decrease of the NMR Knight shift below T_c[10] clearly indicate formation of spin-singlet Cooper pairs. Its superconducting gap was considered to have line nodes from T^3 dependence of the nuclear relaxation rate $1/T_1$ along with the absence of a coherence peak[11–13] and T^2-like temperature dependence of the specific heat[14] in the intermediate-temperature region. These results were considered as evidence of nodal *d*-wave gap symmetry in $CeCu_2Si_2$, such as $d_{x^2-y^2}$ and d_{xy} types.[15,16]

However, from our recent specific-heat study,[17] $CeCu_2Si_2$ has been indicated to be in a full-gap superconducting state with multiband character. Particularly, the H-linear behavior in the low-temperature specific heat and its isotropic field-angle dependence under a rotating magnetic field within the *ab* plane are in sharp contrast to the expected nodal *d*-wave superconductivity. Moreover, in the high-field superconducting state, unusual features have been found in both the magnetization and specific-heat data, suggesting anomalous pair breaking by magnetic field. For instance, both H_{c2} and diamagnetic shielding are unusually reduced on cooling and the low-temperature specific heat is oddly enhanced near H_{c2} (hereafter referred to as "high-field anomaly").

In this paper, we present the results of specific-heat C and magnetization M measurements in order to uncover the origin of the high-field anomaly and to further investigate the gap structure. Qualitatively, both $C(T,H)$ and $M(T,H)$ exhibit the same anomalous behavior for two field directions, $H \parallel a$ and $H \parallel c$. More specifically, the high-field anomaly appears close to H_{c2} below about 0.15 K, and is apparently more distinct in $H \parallel c$ than in $H \parallel a$. From the obtained data, standard thermodynamic parameters are evaluated and possible origins of the high-field anomaly are discussed. From field-angle

dependences of the low-temperature specific heat measured in a rotating magnetic field within the ab and ac planes, we establish that gap nodes are absent at least on heavy-mass bands. We also perform microscopic calculations and clarify that a multiband full-gap model gives reasonable explanation of the power-law-like temperature variation of $C(T)$ and $T_1^{-1}(T)$ in the intermediate-temperature region, the behaviors which had been so far regarded as circumstantial evidence for the presence of line nodes in the gap.

II. EXPERIMENTAL

Single crystals of the S-type $CeCu_2Si_2$ were grown by the flux method.[9] A high-quality single crystal, the same sample as in Ref. 17, was used in this study. The sample mass is 13.4 mg weight and the dimensions are approximately 1, 2, and 1 mm along the crystalline a, b, and c axes, respectively. The dc magnetization was measured down to below 0.07 K by using a high-resolution capacitive Faraday magnetometer[18] in a dilution refrigerator (Oxford Kelvinox25), which was inserted into a superconducting magnet generating a maximum field of 150 kOe with a vertical field gradient of 500 Oe/cm. The specific heat was measured by the standard quasi-adiabatic heat-pulse method or the relaxation method in a dilution refrigerator (Oxford Kelvinox AST Minisorb) down to 0.04 K. This refrigerator was inserted into the vector-magnet system that is composed of a vertical solenoid coil (up to 30 kOe), a horizontal split-pair coil (up to 50 kOe), and a stepper motor mounted at the top of the Dewar to rotate the refrigerator around the vertical axis. By using this system, the field orientation was controlled three-dimensionally with high accuracy of ~ 0.01 deg.

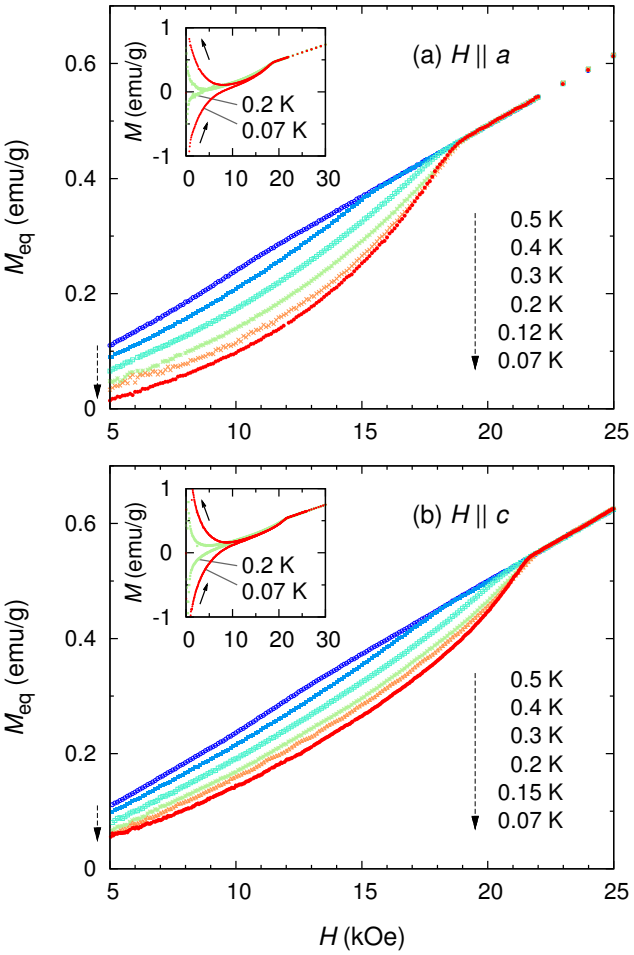

FIG. 1: (Color online) Magnetic field dependence of the equilibrium magnetization M_{eq} at various temperatures in (a) $H \parallel a$ and (b) $H \parallel c$. Insets show raw magnetization curves measured at 0.07 and 0.2 K.

III. RESULTS

A. Magnetization

Raw magnetization data $M(H)$ measured at low temperatures are plotted in the insets of Figs. 1(a) and 1(b) for $H \parallel a$ and $H \parallel c$, respectively. All magnetization curves presented here were taken after zero-field cooling from a temperature well above T_c. In low fields, ordinary magnetization hysteresis due to vortex pinning is observed, which disturbs the detection of the lower critical field H_{c1} (~ 20 Oe).[19] By contrast, in the high-field region ($H \gtrsim 10$ kOe), irreversibility of the magnetization is negligibly small, suggesting the inclusion of defects in the present sample is small. This hysteresis is suppressed significantly with increasing temperature.

To examine the behavior of the equilibrium magnetization, we averaged the $M(H)$ data in the increasing- and decreasing-field sequences. The resulting equilibrium magnetization, labelled as M_{eq}, is plotted for several temperatures in Fig. 1(a) for $H \parallel a$ and Fig. 1(b) for $H \parallel c$. Superconducting signature can be significantly detected in addition to the prominent paramagnetic contribution $\chi_n H$. In order to extract the superconducting contribution, enlarged views of $M_{eq} - \chi_n H$ near H_{c2} are shown in Figs. 2(a) and 2(b) for $H \parallel a$ and $H \parallel c$, respectively. In these figures, the applied magnetic field is normalized by H_{c2} at $T = 0.07$ K, i.e., 19 kOe for $H \parallel a$ and 21.6 kOe for $H \parallel c$.

With decreasing temperature, the shielding becomes pronounced below $\sim 0.95 H_{c2}$ accompanied by a significant increase of the slope of $M_{eq}(H)$ near H_{c2}. The latter feature can be more clearly confirmed from development of a peak height in the field-derivative data in Figs. 2(c) and 2(d). Close inspection of the figures reveals that the onset of superconductivity, H_{c2}, is slightly decreasing on cooling below 0.15 K. This tendency has already been reported from resistivity measurements.[15,20] Our magnetization data provide first thermodynamic evidence for this phenomenon. In particular, the reduction of H_{c2} on cooling below 0.15 K is manifested in the crossing of the $M_{eq}(H)$ curves for $T = 0.07$ and 0.15 (0.12) K below

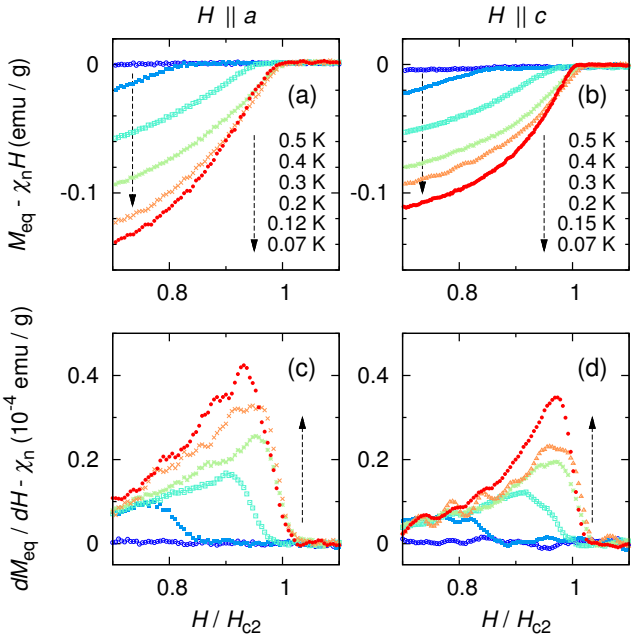

FIG. 2: (Color online) Field dependence of the magnetization at several temperatures, where the paramagnetic contribution is subtracted, for (a) $H \parallel a$ and (b) $H \parallel c$. (c), (d) Differential-susceptibility data obtained from (a) and (b), respectively. In all the figures, the magnetic field is normalized by H_{c2} at 0.07 K.

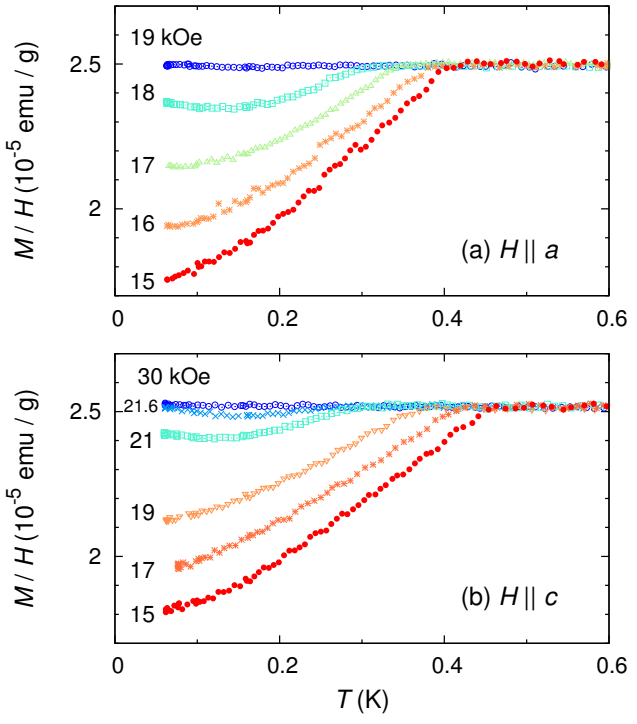

FIG. 3: (Color online) Temperature dependence of M/H in the zero-field-cooling process for (a) $H \parallel a$ and (b) $H \parallel c$.

H_{c2}. This feature is more clearly seen in $H \parallel c$ than in $H \parallel a$.

Temperature dependence of the magnetization shown in Fig. 3 also exhibits unusual behavior at low temperatures in high fields. These data were taken after zero-field cooling, although in this field range $M(T)$ taken in field cooling gives almost the same result, as can be assured by the small hysteresis of $M(H)$ in the high-field region (see the insets of Fig. 1). Under moderate magnetic fields well below H_{c2}, e.g., at 15 kOe, M/H exhibits a monotonic decease on cooling. By contrast, in high fields slightly below H_{c2}, $M(T)$ oddly increases at low temperatures below about 0.15 K, resulting in a distinct minimum near 0.15 K. These results suggest that anomalous pair breaking is operative at low temperatures, particularly for $T \lesssim 0.15$ K near H_{c2}.

B. Specific heat

Figures 4(a) and 4(b) show temperature dependence of the specific-heat data, C_e/T, measured at various magnetic fields applied parallel to the a and c axes, respectively. In all the C_e data, the nuclear contribution, $C_n = (7.4H^2 + 0.1)/T^2$ μJ/(mol K), is subtracted.[17] The normal-state C_e/T, obtained at 19 and 22 kOe for $H \parallel a$ and c, respectively, shows a gradual increase on cooling, which probably originates from three-dimensional spin-density-wave fluctuations in the vicinity of an antiferromagnetic quantum critical point.[14,21]

In zero field, a sharp superconducting transition is observed at $T_c = 0.6$ K with a specific-heat jump of $1.25\gamma T_c$, where the Sommerfeld coefficient γ (= 0.67 J mol^{-1} K^{-2}) is estimated by the C_e/T value at 0.65 K. The inset of Fig. 4(a) shows a semi-log plot of $C_e/\gamma T_c$ against T_c/T. It is clear that the low-temperature $C_e(T)$ data ($T_c/T \gtrsim 5$) can be well fitted by the conventional BCS expression $C(T) = A\exp(-\Delta_0/T) + \gamma_0 T$ (dashed line in the same inset). We confirmed that any power-law temperature functions, by contrast, do not adequately explain the low-temperature $C_e(T)$ data. These facts imply the absence of nodes in the superconducting gap. From the low-temperature fit, a small gap size Δ_0 of 0.39 K is obtained, indicating multiband full-gap superconductivity. The analysis yields a small residual value of $\gamma_0 = 0.028$ J/(mol K^2), which would be attributed to a small amount of inclusions of the non-superconducting A-type $CeCu_2Si_2$ in the sample.

In a weak magnetic field (~ 8 kOe), $C_e(T)/T$ exhibits a rapid decrease on cooling below 0.06 K for both $H \parallel a$ and $H \parallel c$. This feature implies suppression of a minor gap. Above ~ 12 kOe, on the other hand, $C_e(T)/T$ shows an unusual increase on cooling below 0.15 K. Very interestingly, for $H \gtrsim 0.9H_{c2}$, C_e/T exceeds the normal-state value at low temperatures, although the system is definitely in the superconducting state as evidenced by the jump in $C_e(T)$ near 0.3 K. Note that this low-temperature overshoot is specific to the superconducting

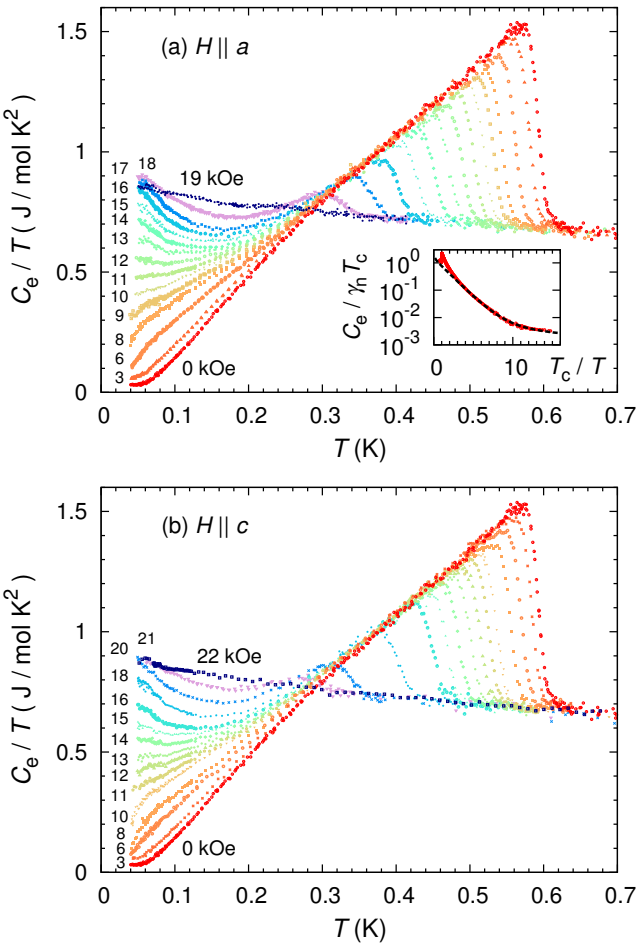

FIG. 4: (Color online) Temperature dependence of C_e/T at various fields in (a) $H \parallel a$ and (b) $H \parallel c$. Here, the nuclear specific-heat contribution is subtracted. Inset in (a) is a semi-log plot of the zero-field $C_e(T)$ data. The dashed line is a fit by using the BCS function in the low-temperature regime.

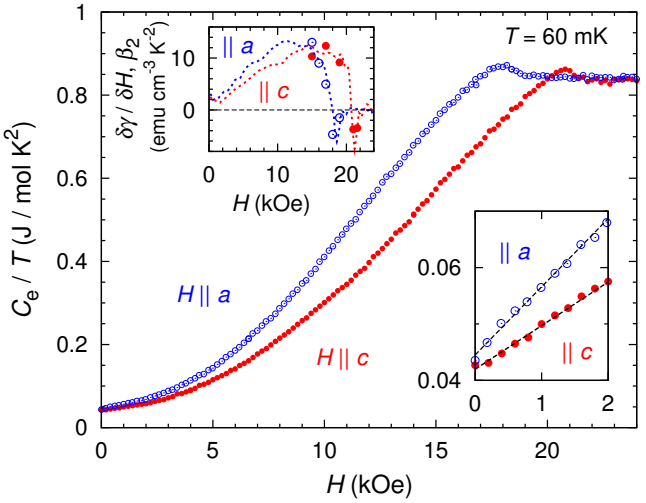

FIG. 5: (Color online) Field dependence of C_e/T at 60 mK for $H \parallel a$ (open) and $H \parallel c$ (closed). Lower inset shows an enlarged plot in the low-field regime. Upper inset shows the slope of $C_e(H)/T$ ($\delta\gamma/\delta H$; dashed lines) and the coefficient of the T^2 term in the $M(T,H)$ data (β_2; circles).

state and disappears above H_{c2}.

Figure 5 plots field dependence of the low-temperature C_e/T measured at 0.06 K for $H \parallel a$ and $H \parallel c$. In the low-field region, $C_e(H)$ increases linearly with magnetic field in both field orientations, as clearly seen in the lower inset of Fig. 5. In the intermediate-field region, $C_e(H)$ exhibits upward curvature and shows a peak slightly below H_{c2}. These features are also confirmed in the field derivative data of $C_e(H)/T$, labelled as $\delta\gamma/\delta H$, shown in the upper inset of Fig. 5 by dashed lines. Qualitatively the same $C_e(H)$ behavior is observed in $H \parallel a$ and $H \parallel c$.

In the low-field limit, the slope of $C_e(H)/T$ is estimated to be 0.012 and 0.007 J/(mol K^2 kOe) for $H \parallel a$ and $H \parallel c$, respectively, as represented by dashed lines in the lower inset of Fig. 5. This H-linear dependence is in sharp contrast to the $\sqrt{H}$ behavior predicted for nodal superconductors,[22] but it is compatible with the expectation for full-gap superconductors as discussed below.

When a superconducting gap is fully open, the quasiparticle density of states increases proportionally with the number of vortex cores, leading to $C_e \propto H$ nearly up to H_{c2}. From microscopic calculations in the $T \to 0$ limit, $dC_e/dH|_{H\sim 0} \sim [C_e(H_{c2}^{orb}) - C_e(0)]/(0.8H_{c2}^{orb})$ has been predicted for an isotropic superconductor,[23,24] where H_{c2}^{orb} is an orbital-limiting field. According to this relation, the observed initial slope implies $H_{c2}^{orb} \sim 84$ (140) kOe for $H \parallel a$ ($H \parallel c$). The result that $H_{c2}^{orb} \gg H_{c2}$ indicates the presence of a strong Pauli paramagnetic effect as discussed in more detail in section IV-B.

One might suspect the possibility that the gradual initial slope in $C_e(H)$ can be attributed to dirty nodal superconductivity; in general, the initial slope of the $\sqrt{H}$ behavior in $C_e(H)$ of nodal superconductors is easily suppressed by the thermal effect as well as the impurity-scattering effect.[25] However, these effects would simultaneously cause significant enhancement of γ_0, which is not in the case of the present sample.

To obtain further evidence for nodeless superconductivity, we investigate the field-angle dependence of the low-temperature C_e. If nodes exist, the quasiparticle density of states, which can be detected from the low-temperature C_e, should oscillate in a rotating magnetic field and show a local minimum when the magnetic field points along a nodal direction.[26,27] This is because quasiparticle excitations caused by the Doppler shift, $\delta E \propto \boldsymbol{v}_F \cdot \boldsymbol{v}_s$, are drastically suppressed at the node where $\boldsymbol{v}_F \perp \boldsymbol{v}_s$. Here, $\boldsymbol{v}_F$ is the Fermi velocity and $\boldsymbol{v}_s$ is the supercurrent velocity circulating around vortices ($\boldsymbol{H} \perp \boldsymbol{v}_s$). Thus, the location of nodes can be detected from field-angle resolved specific-heat measurements.

We have first searched for vertical line nodes from the ϕ-rotation experiment. In Figs. 6(a) and 6(b), we plot $C_e(\phi)/T$ measured in magnetic fields rotated within the

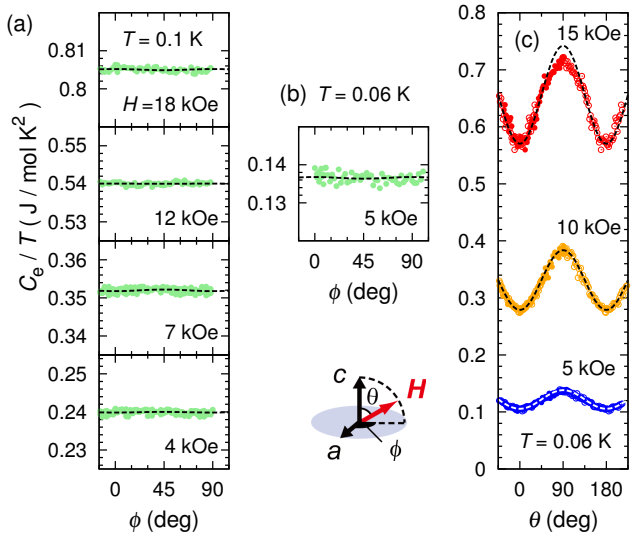

FIG. 6: (Color online) Field angle ϕ dependence of C_e/T measured under a rotating magnetic field within the ab plane at (a) 0.1 and (b) 0.06 K. Here, ϕ is an azimuthal angle between the magnetic field and the a axis. Dashed lines are fits to the data using $C_e(\phi) = C_0 + C_H[1 - A_4\cos(4\phi)]$, where C_0 and C_H are the zero-field and field-dependent parts of C_e. (c) Field-angle-resolved C_e/T at 0.06 K in a magnetic field rotated within the ac plane ($\phi = 90$ deg) as a function of the field angle θ measured relative to the c axis, as illustrated in the center-bottom inset. For clarity, the data measured in the interval $-30° \le \theta \le 100°$ (solid symbols) are plotted repeatedly (open symbols; θ is converted to $-\theta$ and $180° - \theta$).

ab plane at 0.1 and 0.06 K, respectively, where the azimuthal field angle ϕ is measured relative to the a axis. No oscillation that can be ascribed to anisotropic quasiparticle excitations is detected in $C_e(\phi)$ within the resolution of the present experiment. These results support the absence of vertical line nodes that should be expected for $d_{x^2-y^2}$- and d_{xy}-wave types.

Next, in order to examine the presence of horizontal line nodes, we investigate polar field-angle θ dependence of C_e/T in a rotating field within the ac plane at 0.06 K, as shown in Fig. 6(c). Here, θ denotes the angle between the magnetic field and the c axis. Recent investigations have shown that if horizontal line nodes are present, $C_e(\theta)$ is expected to exhibit a local minimum along the nodal direction and a shoulder-like or hump anomaly at certain θ tilted away from the nodal direction at low fields.[28–30] Nevertheless, $C_e(\theta)$ below 10 kOe does not show such features, as represented by dashed lines in Fig. 6(c); the data can be fitted satisfactorily by using a simple twofold function, $C(\theta, H) = A_2(H)\cos 2\theta + C_0(H)$, expected to arise from the tetragonal symmetry. Although a slight deviation from this twofold function is seen in $C_e(\theta)$ at 15 kOe, it is attributable to the anisotropy of H_{c2}; the slope of $C_e(H)$ at 15 kOe is suppressed for $H \parallel a$ whereas it is not yet for $H \parallel c$, as can be confirmed in the upper inset of Fig. 5. Thus, the absence of horizontal line nodes is also well established from the θ-rotation experiment.

IV. DISCUSSION

A. Thermodynamic relations

The superconducting condensation energy $H_c^2/8\pi$ can be evaluated from magnetization and specific-heat data by using the following relations:

$$\frac{H_c^2}{8\pi} = -\int_0^{H_{c2}} [M_{eq}(H) - M_n(H)]dH \quad (1)$$

$$= \int_T^{T_c} dT' \int_{T'}^{T_c} \frac{C_{e,sc}(T'') - C_{e,n}(T'')}{T''} dT'' \quad (2)$$

Here, H_c is the thermodynamic critical field, M_n is the normal-state magnetization, and $C_{e,sc}$ ($C_{e,n}$) is the electronic specific heat of the zero-field superconducting state (normal state above H_{c2}). By assuming $M_n(H) = \chi_n H$, H_c is determined at each temperature from the $M_{eq}(H)$ data and its temperature dependence is plotted in Fig. 7(a) by circles for $H \parallel a$ and squares for $H \parallel c$. Likewise, $H_c(T)$ derived from the zero-field specific-heat data is represented in Fig. 7(a) by a dashed line. These $H_c(T)$ curves obtained from different measurements coincide well at least above 0.1 K. This fact ensures that the present thermodynamic measurements are fully consistent with each other and supports the absence of magnetic transitions below H_{c2}, i.e., $M_n(H) = \chi_n H$. This fact strongly suggests that the high-field anomaly has a superconducting origin. Unfortunately, at the lowest temperature of 0.07 K, H_c could not be evaluated accurately from $M_{eq}(H)$ because of the large vortex-pinning effect in the low-field region.

According to the thermodynamic Maxwell relation, the specific heat and the magnetization must satisfy

$$\frac{\delta}{\delta H}\frac{C(T,H)}{T} = \frac{\delta^2}{\delta T^2}M(T,H). \quad (3)$$

Here, we examine this relation between the present thermodynamic experiments at low temperatures. The left side of eq. (3) can be replaced by the field-derivative C_e/T data at 0.06 K, i.e., $\delta\gamma/\delta H$ already shown in the upper inset of Fig. 5 by dashed lines. To evaluate the right side, temperature dependence of the magnetization [Figs. 3(a) and 3(b)] is fitted by using a function $M(T,H) = M_0(H) + \frac{1}{2}\beta_2(H)T^2$ in the temperature range below 0.12 K, and the resulting field variation of β_2 is represented by circles in the upper inset of Fig. 5. Equation (3) can then be reduced to $\delta\gamma/\delta H = \beta_2$. A good agreement between $\delta\gamma/\delta H$ and β_2 further strengthens reliability of the present thermodynamic experiment and ensures the occurrence of the superconducting anomaly in high magnetic fields.

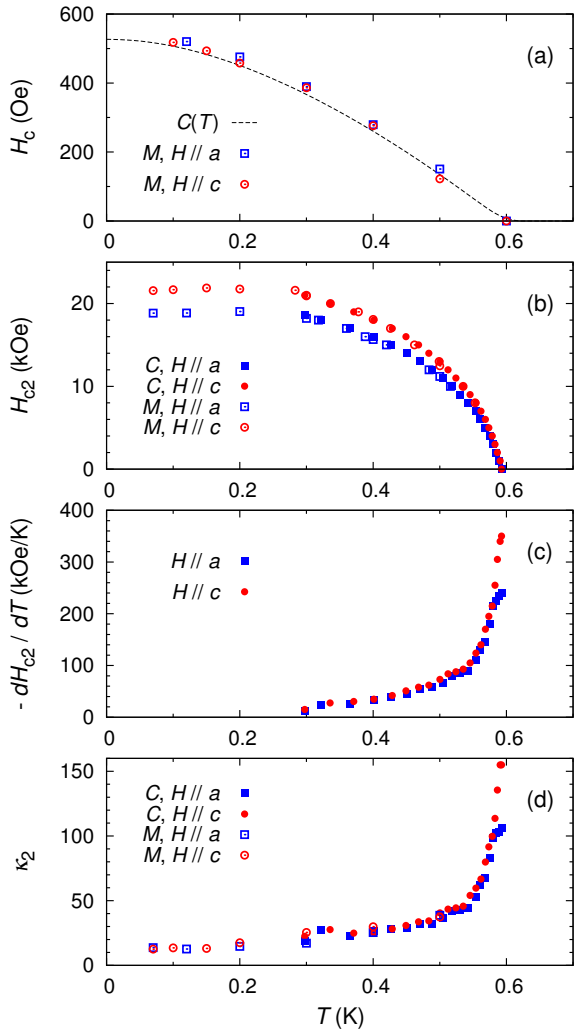

FIG. 7: (Color online) Temperature dependences of (a) the thermodynamic critical field H_c, (b) the upper critical field H_{c2}, (c) the slope of $H_{c2}(T)$, and (d) the Maki parameter κ_2. determined from specific-heat and the magnetization measurements.

B. Limit of the upper critical field

The H-T phase diagram determined from the present $C_e(T,H)$ and $M(T,H)$ data is shown in Fig. 7(b). The results are consistent with previous studies[15,20] and exhibit strong limit of H_{c2} at low temperatures in both field directions; in particular, the strange decrease of H_{c2} below ~ 0.2 K, already reported from resistivity measurements,[15,20,31] is detected by the present thermodynamic measurements as well. It has been proposed that this phenomenon is related to the A phase; superconductivity and the A phase order compete each other.[31]

By using the data in Fig. 7(b), we plot temperature dependence of $-dH_{c2}/dT$ in Fig. 7(c). The initial slope of $H_{c2}(T)$ at T_c is roughly -240 kOe/K for $H \parallel a$ and -350 kOe/K for $H \parallel c$. On the basis of the Werthamer-Helfand-Hohenberg theory,[32,33] the orbital-limiting field can be given by $H_{c2}^{\rm orb} \sim -0.7T_c dH_{c2}/dT|_{T_c}$. By using this formula, $H_{c2}^{\rm orb}$ is estimated to be 100 kOe for $H \parallel a$ and 147 kOe for $H \parallel c$. These values are in good agreements with those evaluated from the full-gap analysis of the $C_e(H)$ data in section III-B. These $H_{c2}^{\rm orb}$ values, $\gtrsim 5$ times higher than the observed H_{c2}, demonstrate the existence of a strong pair-breaking mechanism under magnetic fields in $CeCu_2Si_2$.

In order to further characterize the pair-breaking effect, we evaluate the Ginzburg-Landau parameter κ_2 by using the following expressions:

$$\left.\frac{d(M_{\rm eq}-\chi_n H)}{dH}\right|_{H_{c2}} = \frac{1}{4\pi\beta(2\kappa_2^2-1)} \qquad (4)$$

and

$$\left.\frac{\Delta C}{T}\right|_{T_c} = \left(\frac{dH_{c2}}{dT}\right)^2 \frac{1}{4\pi\beta(2\kappa_2^2-1)}. \qquad (5)$$

Here, ΔC is the jump of the specific heat at $T_c(H)$ taken from Figs. 4(a) and 4(b). The parameter β is assumed to be 1.16 for a triangular vortex lattice. The obtained $\kappa_2(T)$ is plotted in Fig. 7(d) as a function of T; κ_2 shows a rapid decrease on cooling near T_c and becomes constant at low temperatures.

A rapid decrease of κ_2 near T_c is reminiscent of the strong Pauli-paramagnetic effect. A parameter α is introduced to characterize the Pauli-paramagnetic effect, and it is defined by $\alpha = \sqrt{2}H_{c2}^{\rm orb}(0)/H_P(0)$, where $H_P(0)$ denotes the Pauli limiting field at $T = 0$: the upper critical field solely determined by the paramagnetic depairing effect. For a single-band Pauli-limited superconductor with $\alpha > 1$, it is expected that κ_2 decreases rapidly near T_c and crosses zero at a finite temperature. Below this temperature, the superconducting-normal transition at H_{c2} becomes first order. In the case of a strong Pauli-paramagnetic limit $\alpha \gg 1$, the transition at H_{c2} remains first order up to $\simeq 0.58T_c$.[34]

The steep decrease of κ_2 below T_c in Fig. 7(d) suggests $\alpha \gg 1$. Nevertheless, $\kappa_2(T)$ levels off below 0.5 K and does not cross zero. The absence of the first-order transition in $CeCu_2Si_2$ is apparently inconsistent with the conventional Pauli-limited scenario. We propose the unusual Pauli-paramagnetic effect to provide further support for multiband superconductivity in $CeCu_2Si_2$.[17] Indeed, the anomalous temperature dependence of κ_2 can be explained by a minimal two-band model for a Pauli-limited superconductor,[35] whose mechanism is intuitively explained as follows. We define the orbital limiting field and the Pauli limiting field of band i ($i = 1, 2$) as $H_{c2}^{{\rm orb}(i)}$ and $H_P^{(i)}$, respectively. Assume $H_{c2}^{{\rm orb}(2)} > H_{c2}^{{\rm orb}(1)}$ and $H_P^{(1)} > H_P^{(2)}$, so that band 2 alone exhibits a first-order transition at low T. The actual H_{c2} near T_c is governed by $H_{c2}^{{\rm orb}(2)}$ and is subject to the strong paramagnetic effect, leading to a steep decrease in $\kappa_2(T)$. As the temperature further decreases, $H_{c2}^{(2)}(T)$ of band 2 is more

suppressed than $H_{c2}^{(1)}(T)$ of band 1 and eventually becomes $H_{c2}^{(2)}(T) < H_{c2}^{(1)}(T)$. At low temperatures, therefore, the actual H_{c2} is determined by $H_{c2}^{(1)}(T)$ and the otherwise first-order transition of band 2 is hindered. Microscopic calculations based on the quasiclassical Eilenberger equations provide theoretical basis of the above argument.[35] Moreover, the calculations can also explain the low-temperature anomaly in $M(T)$ (Fig. 3) and C/T (Figs. 4 and 5) at high fields as a consequence of the edge singularity of the band-2 gap. We note that a similar field-induced anomaly has been observed in the specific heat of KFe_2As_2,[36] which also exhibits multiband superconductivity with strong Pauli-limiting behavior.[37,38]

C. Gap symmetry

Temperature dependence of the specific heat suggests the presence of at least two fully-open gaps in $CeCu_2Si_2$. Multiband nature of $CeCu_2Si_2$ has also been supported by the recent results of the scanning tunneling microscope experiment.[39] Furthermore, dependences of the low-temperature specific heat on magnetic field and its orientation have indicated the deficiency of nodal quasiparticle excitations. On the basis of these results, it is most plausible that $CeCu_2Si_2$ is a full-gap superconductor. However, the presence of nodes on light-mass bands cannot be ruled out completely only from the present study because the specific heat is dominated by heavy-mass quasiparticles. Therefore, identification of the gap structure by using other techniques is important, such as thermal-conductivity measurements and penetration depth measurements, which are powerful probes to detect light-mass quasiparticles excited from light-mass bands.

Another possibility to be considered is that the Fermi surface is absent at the locations where the gap function has nodes. Under such a situation, nodal quasiparticles would be totally missing. According to the recent band-structure calculations on $CeCu_2Si_2$,[17,40] one electron band with the heaviest mass exists around the X point, and two hole bands with relatively light mass are present around the Z point. Based on this Fermi-surface topology along with two-band full-gap nature of superconductivity, possibilities of A_{2g} $[k_xk_y(k_x^2-k_y^2)]$, B_{1g} $[k_x^2-k_y^2]$, B_{2g} $[k_{xy}]$ and E_g gap functions can be safely ruled out.

If nodes are indeed absent on any bands, spin-singlet superconductivity in the tetragonal D_{4h} symmetry only allows the gap symmetry of A_{1g}, i.e., a combination of the gap functions: 1, $k_x^2+k_y^2$, k_z^2, etc., including the case of sign-changing A_{1g}. Alternatively, if we consider the possibility of orbital-selective pairing states, a fully-gapped "$d_{x^2-y^2}+d_{xy}$" band-mixing state might be another candidate, which has been recently proposed.[41] Such gap symmetries are unprecedented in the heavy-fermion systems, and the elucidation of the pairing mechanism would contribute to deepen the understanding of unconventional superconductivity.

D. Multiband full-gap analyses of $C(T)$ and $T_1^{-1}(T)$

We now turn to the temperature variation of zero-field $C_e(T)$ and $T_1^{-1}(T)$ of $CeCu_2Si_2$. The seeming power-law temperature dependences of these quantities at an intermediate-T range, along with the absence of the coherence peak in $1/T_1$ just below T_c, have been considered as solid evidence for d-wave superconductivity with line of nodes in this material. A question that arises is whether the multiband full-gap model can explain these features as well.

To answer this question, we perform microscopic calculations of the zero-field $C(T)$ and $1/T_1(T)$ by using the quasi-classical Green's functions as follows:[42–44]

$$\frac{(T_1T)^{-1}}{(T_1T)^{-1}_{T=T_c}} = \frac{2}{k_BT}\int_0^\infty \left\{ \left[\sum_i N_i^s(E)\right]^2 + \left|\sum_i M_i^s(E)\right|^2 \right\} f(E)[1-f(E)]dE \tag{6}$$

$$\frac{C}{\gamma_n T} = \frac{6}{\pi^2}\frac{1}{(k_BT)^3}\sum_i \int_0^{2\pi}\frac{d\phi}{4\pi}\int_0^\pi d\theta\sin\theta\int_0^\infty N_i^s(E,\phi,\theta)\left[E^2-\frac{T}{2}\frac{d|\Delta_i(\phi,\theta)|^2}{dT}\right]f(E)[1-f(E)]dE. \tag{7}$$

Here, the density of states is described by

$$N_i^s(E) = \int_0^{2\pi}\frac{d\phi}{4\pi}\int_0^\pi d\theta\sin\theta N_i^s(E,\phi,\theta) \tag{8}$$

$$N_i^s(E,\phi,\theta) = n_i^s \mathrm{Re}\left[\frac{-i(E+i\eta)}{\sqrt{|\Delta_i(\phi,\theta)|^2-(E+i\eta)^2}}\right] \tag{9}$$

and the anomalous density of states arising from the co-

herence effect is written as

$$M_i^{\rm s}(E) = \int_0^{2\pi} \frac{d\phi}{4\pi} \int_0^{\pi} d\theta \sin\theta M_i^{\rm s}(E,\phi,\theta) \quad (10)$$

$$M_i^{\rm s}(E,\phi,\theta) = n_i^{\rm s}\Delta_i(\phi,\theta){\rm Im}\left[\frac{1}{\sqrt{|\Delta_i(\phi,\theta)|^2-(E+i\eta)^2}}\right]. \quad (11)$$

The smearing factor η is introduced when $1/T_1$ is calculated ($\eta = 0$ when C is calculated). The parameter n_i denotes the weight of the i-th band. In the present analyses, a two-band full-gap model is used for simplicity; two superconducting gaps $\Delta_i(\phi,\theta)$ ($i = 1$ and 2) are assumed to be independent of ϕ and θ. Temperature dependence of Δ_i is obtained by solving the gap equation at each temperature.

First, we focus on model A in Table I which was proposed in the previous report.[17] As shown in Fig. 8(a), $C/\gamma T$ of model A (solid line) can reproduce sufficiently the modified zero-field specific-heat data, $[C_{\rm e}(T, 0\ {\rm T}) - C_{\rm e}(T, 3\ {\rm T})]/\gamma^* T + 1$ (open circles), which satisfy entropy balance in the BCS framework; the temperature-dependent part in the normal-state $C_{\rm e}/T$ is embedded in the superconducting $C_{\rm e}/T$ by subtracting the data at 3 T for $H \parallel a$.[17] Here, γ^* is equal to $C_{\rm e}(3\ {\rm T}) - C_{\rm e}(0\ {\rm T})$ at $T \to 0$ ($= 0.84$ J mol^{-1} K^{-2}). This result demonstrates that the two-band full-gap model is not inconsequent for $CeCu_2Si_2$.

Next, we calculate $1/T_1(T)$ by using the same parameters of model A. Calculated results of $1/T_1(T)$ for $\eta/k_{\rm B}T_{\rm c} = 0.01$ and 0.1 are represented in Fig. 8(b) by solid and dashed lines, respectively. Experimental data of $1/T_1(T)$, shown in the same figure by circles, are taken from the previous report[12] on polycrystalline S-type $CeCu_{2.05}Si_2$. In the high-temperature region below $T_{\rm c}$, a clear enhancement of $1/T_1$, i.e., a coherence peak, appears clearly in the calculated result for $\eta/k_{\rm B}T_{\rm c} = 0.01$. Although this enhancement is suppressed by increasing η, the calculated $1/T_1$ for $\eta/k_{\rm B}T_{\rm c} = 0.1$ is still larger than the experimental result in wide temperature range.

In order to reproduce the strong reduction of $1/T_1$ just below $T_{\rm c}$, both Δ_1 and Δ_2 are increased in model B. Then, the calculated result [solid line in Fig. 8(d)] agrees approximately with the experimental result. Here, we adopt $\eta/k_{\rm B}T_{\rm c} = 0.1$. This increase of Δ_i leads to a larger specific-heat jump at $T_{\rm c}$. In Fig. 8(c), the calculated $C/\gamma T$ by model B is shown by a solid line. The specific-heat jump, $\Delta C/\gamma T$, calculated by model B is 1.4 whereas $\Delta C/\gamma T = 1.0$ by model A. However, $\Delta C/\gamma T = 1.4$ matches better with the jump in the experimental $C_{\rm e}/\gamma T$ shown in Fig. 8(c) by circles; a jump in the modified specific-heat data [open circles in Fig. 8(a)] is underestimated because of $\gamma^* > \gamma$. Thus, the gap sizes in model B are quantitatively reasonable to reproduce $C_{\rm e}(T)$ as well.

Model	$\Delta_1/k_{\rm B}T_{\rm c}$	$\Delta_2/k_{\rm B}T_{\rm c}$
A	1.76	0.7
B	2.1	0.8
C	2.1	-0.8

TABLE I: Superconducting gaps Δ_i ($i = 1$ and 2) used in the present two-band full-gap analyses. In all the models, weights of primary (Δ_1) and secondary (Δ_2) bands are 65% and 35% of the total density of states, respectively, i.e., $n_1 = 0.65$ and $n_2 = 0.35$.

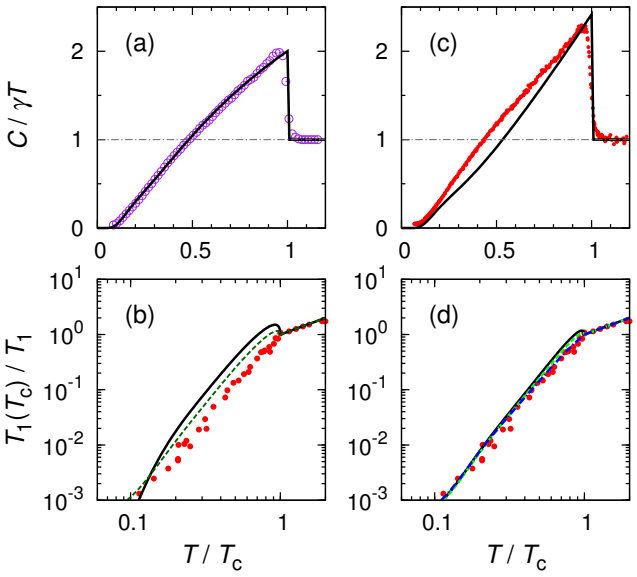

FIG. 8: (Color online) Two-band full-gap analyses of (a) $C(T)$ and (b) $1/T_1(T)$ by using model A. Analyses of (c) $C(T)$ and (d) $1/T_1(T)$ by using models B and C. The calculated results are represented by lines. Solid circles in (c) are experimental data of $C_{\rm e}/\gamma T$. Open circles in (a) represent modified specific-heat data, $[C_{\rm e}(T, 0\ {\rm T}) - C_{\rm e}(T, 3\ {\rm T})]/\gamma^* T + 1$, which was introduced in Ref. 17. Circles in (b) and (d) are experimental data of $1/T_1$ taken from the previous report[12] on polycrystalline $CeCu_{2.05}Si_2$. Solid and dashed lines in (b) represent the calculated results with $\eta/k_{\rm B}T_{\rm c} = 0.01$ and 0.1, respectively. Solid and dashed lines in (d) are the calculated results by models B and C with $\eta/k_{\rm B}T_{\rm c} = 0.1$, respectively. Models B and C provide the same results of $C(T)$. A dot-dashed line in (d) is the calculated result by model C with temperature-dependent smearing factor, $\eta(T)/k_{\rm B}T_{\rm c} = 0.1 + 0.5(T/T_{\rm c})^2$.

Finally, in order to examine a possibility of $s_\pm$ superconductivity, we here adopt model C in which signs of two gaps are opposite. Calculated result of $1/T_1(T)$ by model C is shown in Fig. 8(d) by a dashed line; the coherence peak is slightly suppressed compared with that of the s_{++} model (solid line, model B). Nevertheless, difference between them is not so significant. This is because the term $M_1^{\rm s}(E)M_2^{\rm s}(E)$, which makes the difference between $s_\pm$ and s_{++}, is not large for the present parameters. Note that $C(T)$ calculated by model C is the same as that by model B because the gap amplitude, which is the same for both cases, governs the calculated $C(T)$. These results suggest that both $s_\pm$ and s_{++} models are allowed

for $CeCu_2Si_2$.

The lack of the coherence peak in the experimental $1/T_1$, which cannot be fully reproduced even by models B and C, might be due to some damping of quasiparticles. Indeed, strong quasiparticle damping is possible in $CeCu_2Si_2$ particularly near T_c because inelastic spin fluctuations, a good candidate of the pairing interaction, are enhanced by temperature roughly proportional to T^2.[8] If we assume that η also increases proportionally to T^2 up to T_c, reflecting the temperature-dependent pairing interaction, a coherence peak almost diminishes, as demonstrated in Fig. 8(d) by a dot-dashed line [model C with $\eta(T)/k_BT_c = 0.1 + 0.5(T/T_c)^2$]. Thus, the behavior of $1/T_1(T)$, reminiscent of nodal superconductivity, can be explained reasonably in the framework of a multiband full-gap model.

V. SUMMARY

We have performed low-temperature magnetization and specific-heat measurements on a high-quality single crystal of the S-type $CeCu_2Si_2$. The high-field anomaly in the superconducting state has been detected from both thermodynamic measurements that satisfy standard thermodynamic relations. It has been revealed that this anomaly becomes prominent below roughly 0.15 K and occurs more abrupt near H_{c2} in $H \parallel c$. From azimuthal and polar field-angle dependences of the low-temperature specific heat, the absence of vertical and horizontal line nodes in the superconducting gap on heavy-mass bands has been established. We have also demonstrated that a two-band full-gap model can reproduce temperature dependences of the zero-field $C_e(T)$ and $1/T_1(T)$ in the wide temperature range, which had been considered to be hallmarks of nodal superconductivity. These results help establish multiband full-gap superconductivity of $CeCu_2Si_2$.

Acknowledgments

We thank K. Ishida for providing us experimental data of $1/T_1$ and giving fruitful discussion. This work was supported by a Grant-in-Aid for Scientific Research on Innovative Areas "J-Physics" (15H05883) from MEXT, and KAKENHI (15K05158, 15H03682, 26400360, 15H05745, 15K17715, 15J05698) from JSPS.

[1] T. Sakakibara, S. Kittaka, and K. Machida, Rep. Prog. Phys. **79**, 094002 (2016).
[2] K. Izawa, H. Yamaguchi, Y. Matsuda, H. Shishido, R. Settai, and Y. Onuki, Phys. Rev. Lett. **87**, 057002 (2001).
[3] K. An, T. Sakakibara, R. Settai, Y. Onuki, M. Hiragi, M. Ichioka, and K. Machida, Phys. Rev. Lett. **104**, 037002 (2010).
[4] T. Park, E. D. Bauer, and J. D. Thompson, Phys. Rev. Lett. **101**, 177002 (2008).
[5] Y. Kasahara, T. Iwasawa, Y. Shimizu, H. Shishido, T. Shibauchi, I. Vekhter, and Y. Matsuda, Phys. Rev. Lett. **100**, 207003 (2008).
[6] S. Kittaka, Y. Aoki, T. Sakakibara, A. Sakai, S. Nakatsuji, Y. Tsutsumi, M. Ichioka, and K. Machida, Phys. Rev. B **85**, 060505 (2012).
[7] F. Steglich, J. Aarts, C. D. Bredl, W. Lieke, D. Meschede, W. Franz, and H. Schäfer, Phys. Rev. Lett. **43**, 1892 (1979).
[8] O. Stockert, J. Arndt, E. Faulhaber, C. Geibel, H. S. Jeevan, S. Kirchner, M. Loewenhaupt, K. Schmalzl, W. Schmidt, Q. Si, and F. Steglich, Nat. Phys. **7**, 119 (2011).
[9] S. Seiro, M. Deppe, H. Jeevan, U. Burkhardt, and C. Geibel, Phys. Status Solidi B **247**, 614 (2010).
[10] K. Ueda, Y. Kitaoka, H. Yamada, Y. Kohori, T. Kohara, and K. Asayama, J. Phys. Soc. Jpn. **56**, 867 (1987).
[11] Y. Kitaoka, K. Ueda, K. Fujiwara, H. Arimoto, H. Iida, and K. Asayama, J. Phys. Soc. Jpn. **55**, 723 (1986).
[12] K. Ishida, Y. Kawasaki, K. Tabuchi, K. Kashima, Y. Kitaoka, K. Asayama, C. Geibel, and F. Steglich, Phys. Rev. Lett. **82**, 5353 (1999).
[13] K. Fujiwara, Y. Hata, K. Kobayashi, K. Miyoshi, J. Takeuchi, Y. Shimaoka, H. Kotegawa, T. C. Kobayashi, C. Geibel, and F. Steglich, J. Phys. Soc. Jpn. **77**, 123711 (2008).
[14] J. Arndt, O. Stockert, K. Schmalzl, E. Faulhaber, H. S. Jeevan, C. Geibel, W. Schmidt, M. Loewenhaupt, and F. Steglich, Phys. Rev. Lett. **106**, 246401 (2011).
[15] H. A. Vieyra, N. Oeschler, S. Seiro, H. S. Jeevan, C. Geibel, D. Parker, and F. Steglich, Phys. Rev. Lett. **106**, 207001 (2011).
[16] I. Eremin, G. Zwicknagl, P. Thalmeier, and P. Fulde, Phys. Rev. Lett. **101**, 187001 (2008).
[17] S. Kittaka, Y. Aoki, Y. Shimura, T. Sakakibara, S. Seiro, C. Geibel, F. Steglich, H. Ikeda, and K. Machida, Phys. Rev. Lett. **112**, 067002 (2014).
[18] T. Sakakibara, H. Mitamura, T. Tayama, and H. Amitsuka, Jpn. J. Appl. Phys. **33**, 5067 (1994).
[19] U. Rauchschwalbe, W. Lieke, C. D. Bredl, F. Steglich, J. Aarts, K. M. Martini, and A. C. Mota, Phys. Rev. Lett. **49**, 1448 (1982).
[20] W. Assmus, M. Herrmann, U. Rauchschwalbe, S. Riegel, W. Lieke, H. Spille, S. Horn, G. Weber, F. Steglich, and G. Cordier, Phys. Rev. Lett. **52**, 469 (1984).
[21] P. Gegenwart, C. Langhammer, C. Geibel, R. Helfrich, M. Lang, G. Sparn, F. Steglich, R. Horn, L. Donnevert, A. Link, and W. Assmus, Phys. Rev. Lett. **81**, 1501 (1998).
[22] G. E. Volovik, JETP Lett. **58**, 469 (1993).
[23] N. Nakai, M. Ichioka, and K. Machida, J. Phys. Soc. Jpn. **71**, 23 (2002).
[24] N. Nakai, P. Miranović, M. Ichioka, and K. Machida, Phys. Rev. B **70**, 100503 (2004).
[25] C. Kübert and P. J. Hirschfeld, Solid State Commun. **105**, 459 (1998).
[26] I. Vekhter, P. J. Hirschfeld, J. P. Carbotte, and E. J. Nicol, Phys. Rev. B **59**, R9023 (1999).

[27] T. Sakakibara, A. Yamada, J. Custers, K. Yano, T. Tayama, H. Aoki, and K. Machida, J. Phys. Soc. Jpn. **76**, 051004 (2007).
[28] S. Kittaka, Y. Shimizu, T. Sakakibara, Y. Haga, E. Yamamoto, Y. Ōnuki, Y. Tsutsumi, T. Nomoto, H. Ikeda, and K. Machida, J. Phys. Soc. Jpn. **85**, 033704 (2016).
[29] Y. Shimizu, S. Kittaka, T. Sakakibara, Y. Tsutsumi, T. Nomoto, H. Ikeda, K. Machida, Y. Homma, and D. Aoki, Phys. Rev. Lett. **117**, 037001 (2016).
[30] Y. Tsutsumi, T. Nomoto, H. Ikeda, and K. Machida, arXiv:1604.02806.
[31] I. Sheikin, D. Braithwaite, J.-P. Brison, A. I. Buzdin, and W. Assmus, J. Phys.: Condens. Matter **10**, L749 (1998).
[32] E. Helfand and N. R. Werthamer, Phys. Rev. **147**, 288 (1966).
[33] N. R. Werthamer, E. Helfand, and P. C. Hohenberg, Phys. Rev. **147**, 295 (1966).
[34] G. Sarma, J. Phys. Chem. Solids **24**, 1029 (1963).
[35] Y. Tsutsumi, K. Machida, and M. Ichioka, Phys. Rev. B **92**, 020502 (2015).
[36] S. Kittaka, Y. Aoki, N. Kase, T. Sakakibara, T. Saito, H. Fukazawa, Y. Kohori, K. Kihou, C. H. Lee, A. Iyo, H. Eisaki, K. Deguchi, N. K. Sato, Y. Tsutsumi, and K. Machida, J. Phys. Soc. Jpn. **83**, 013704 (2014).
[37] P. Burger, F. Hardy, D. Aoki, A. E. Böhmer, R. Eder, R. Heid, T. Wolf, P. Schweiss, R. Fromknecht, M. J. Jackson, C. Paulsen, and C. Meingast, Phys. Rev. B **88**, 014517 (2013).
[38] F. Hardy, R. Eder, M. Jackson, D. Aoki, C. Paulsen, T. Wolf, P. Burger, A. Böhmer, P. Schweiss, P. Adelmann, R. A. Fisher, and C. Meingast, J. Phys. Soc. Jpn. **83**, 014711 (2014).
[39] M. Enayat, Z. Sun, A. Maldonado, H. Suderow, S. Seiro, C. Geibel, S. Wirth, F. Steglich, and P. Wahl, Phys. Rev. B **93**, 045123 (2016).
[40] H. Ikeda, M.-T. Suzuki, and R. Arita, Phys. Rev. Lett. **114**, 147003 (2015).
[41] G. M. Pang, M. Smidman, J. L. Zhang, L. Jiao, Z. F. Weng, E. M. Nica, Y. Chen, W. B. Jiang, Y. J. Zhang, H. S. Jeevan, P. Gegenwart, F. Steglich, Q. Si, H. Q. Yuan, arXiv:1605.04786.
[42] Y. Nagai, N. Hayashi, N. Nakai, H. Nakamura, M. Okumura, and M. Machida, New J. Phys. **10**, 103026 (2008).
[43] F. Bouquet, Y. Wang, R. A. Fisher, D. G. Hinks, J. D. Jorgensen, A. Junod, and N. E. Phillips, EuroPhys. Lett. **56**, 856 (2001).
[44] H. Fukazawa, Y. Yamada, K. Kondo, T. Saito, Y. Kohori, K. Kuga, Y. Matsumoto, S. Nakatsuji, H. Kito, P. M. Shirage, K. Kihou, N. Takeshita, C.-H. Lee, A. Iyo, and H. Eisaki, J. Phys. Soc. Jpn. **78**, 083712 (2009).